Rational Linker Design to Accelerate Excretion and Reduce Background Uptake of Peptidomimetic PSMA-Targeting Hybrid Molecules

Ann-Christin Eder[1–3], Martin Schäfer[1], Jana Schmidt[1], Ulrike Bauder-Wüst[1], Mareike Roscher[1], Karin Leotta[4,5], Uwe Haberkorn[4,5], Klaus Kopka*[1,6], and Matthias Eder*[2,3]

[1]*Division of Radiopharmaceutical Chemistry, German Cancer Research Center (DKFZ), Heidelberg, Germany;* [2]*Department of Nuclear Medicine, University Medical Center Freiburg, Faculty of Medicine, University of Freiburg, Freiburg, Germany;* [3]*Division of Radiopharmaceutical Development, German Cancer Consortium (DKTK), partner site Freiburg, Freiburg, Germany and German Cancer Research Center, Heidelberg, Germany;* [4]*Department of Nuclear Medicine, Heidelberg University Hospital, Heidelberg, Germany;* [5]*Clinical Cooperation Unit Nuclear Medicine, German Cancer Research Center (DFKZ), Heidelberg, Germany; and* [6]*German Cancer Consortium (DKTK), Heidelberg, Germany*

The evolution of peptidomimetic hybrid molecules for preoperative imaging and guided surgery targeting the prostate-specific membrane antigen (PSMA) significantly progressed over the past few years, and some approaches are currently being evaluated for further clinical translation. However, accumulation in nonmalignant tissue such as kidney, bladder, spleen, or liver might limit tumor-to-background contrast for precise lesion delineation, particularly in a surgical setting. To overcome these limitations, a rational linker design aims at the development of a second generation of PSMA-11–based hybrid molecules with an enhanced pharmacokinetic profile and improved imaging contrast. **Methods:** A selection of rationally designed linkers was introduced to the PSMA-targeting hybrid molecule Glu-urea-Lys-HBED-CC-IRDye800CW, resulting in a second-generation peptidomimetic hybrid molecule library. The biologic properties were investigated in cell-based assays. In a preclinical proof-of-concept study with the radionuclide ^{68}Ga, the impact of the modifications was evaluated by determination of specific tumor uptake, pharmacokinetics, and fluorescence imaging in tumor-bearing mice. **Results:** The modified hybrid molecules carrying various selected linkers revealed high PSMA-specific binding affinity and effective internalization. The highest tumor-to-background contrast of all modifications investigated was identified for the introduction of a histidine- (H) and glutamic acid (E)–containing linker ($(HE)_3$-linker) between the PSMA-binding motif and the chelator. In comparison to the parental core structure, uptake in nonmalignant tissue was significantly reduced to a minimum, as exemplified by an 11-fold reduced spleen uptake from 38.12 ± 14.62 percentage injected dose (%ID)/g to 3.47 ± 1.39 %ID/g (1 h after injection). The specific tumor uptake of this compound (7.59 ± 0.95 %ID/g, 1 h after injection) was detected to be significantly higher than that of the parental tracer PSMA-11. These findings confirmed by PET and fluorescence imaging are accompanied by an enhanced pharmacokinetic profile with accelerated background clearance at early time points after injection. **Conclusion:** The novel generation of PSMA-targeting hybrid molecules reveals fast elimination, reduced background organ enrichment, and high PSMA-specific tumor uptake meeting the key demands for potent tracers in nuclear medicine and fluorescence-guided surgery. The approach's efficacy in improving the pharmacokinetic profile highlights the strengths of rational linker design as a powerful tool in strategic hybrid-molecule development.

Key Words: PSMA; hybrid molecules; prostate cancer; guided surgery; pharmacokinetic profile

J Nucl Med 2021; 62:1461–1467
DOI: 10.2967/jnumed.120.248443

Surgical resection of tumor tissue represents one of the main curative treatment options in the clinical management of prostate cancer (*1*). The precise detection and comprehensive resection of malignancies is thereby of high significance for patient survival and therapy success. During resection, several difficulties are limiting the therapeutic outcome. Although malignant tissue can be precisely localized preoperatively using diagnostic radiopharmaceuticals, the translation to the operating theater often remains challenging. This increases the risk that tumor tissue will be missed by the surgeon (*2*,*3*). Additionally, a close proximity of lesions to essential healthy structures such as the urinary bladder or nerves impedes a wide dissection in the lower pelvis, resulting in positive surgical margins (*4*). These difficulties cause an increased possibility of cancer recurrence and subsequent treatment failure (*5*). Consequently, template-based extended lymphadenectomies, for example, are performed to diminish the risk of left-behind lesions (*6*,*7*). Besides malignant tissue, a considerable amount of healthy tissue is removed during this surgical strategy, causing increased morbidity. Hence, there is a strong medical need for advances in the field of intraoperative navigation to precisely delineate tumor tissue from surrounding healthy tissue.

To overcome these issues, novel approaches have been developed over the past few years comprising the detection of malignant tissue supported by both a γ-probe and a fluorescent dye. A combination of these 2 modalities in so-called hybrid or dual-labeled approaches compensates for their respective disadvantages, thereby merging the strengths of both technologies. In a clinical scenario, these novel approaches provide preoperative imaging (e.g., PET/CT) for planning of the surgery, combined with subsequent intraoperative navigation. The first clinical proof-of-concept studies with the indocyanine green–based hybrid sentinel

Received May 1, 2020; revision accepted Jan. 13, 2021.
For correspondence or reprints, contact Ann-Christin Eder (ann-christin.eder@uniklinik-freiburg.de).
*Contributed equally to this work.
Published online March 19, 2021.

lymph node tracer indocyanine green–^{99m}Tc-nanocolloid demonstrated the feasibility of dual-modality approaches to improve surgical accuracy in different cancer types (*8–10*). Because nontargeted approaches have their limitations in precisely detecting tumor tissue, recent advances have focused on the design of targeted dual-modality probes.

For the specific targeting of prostate cancer, the prostate-specific membrane antigen (PSMA) has been identified as an excellent target structure. PSMA is a transmembrane carboxypeptidase that is selectively overexpressed in most prostate carcinomas, including local lesions, malignant lymph nodes, and bone metastases (*11–14*). The first PSMA-targeting dual-modality antibodies and small-molecule peptidomimetic inhibitors have recently demonstrated the feasibility of hybrid detection in preclinical studies (*15–18*). Besides high and specific tumor uptake of targeted hybrid probes, a favorable pharmacokinetic profile with, for example, a low accumulation in off-target tissue, fast clearance, and a resulting high imaging contrast at early time points after injection is crucial for further clinical translation.

With the development of dual-modality low-molecular-weight PSMA inhibitors based on the clinically established PET tracer ^{68}Ga-PSMA-11, a versatile platform was designed tolerating the conjugation of a fluorescent dye combined with a radiolabel moiety (*18–20*). Our theranostic dual-modality platform is thus characterized by high and fast PSMA-specific tumor uptake along with rapid background clearance allowing preoperative imaging combined with intraoperative guidance (*18*). The advantageous effect of introducing spacer moieties comprising histidine (H) and glutamic acid (E) on the biodistribution profile of Affibody (Affibody AB) molecules was originally reported by Hofstrom et al. (*21*). Further work from our group successfully established (HE)$_3$ linker modifications to PSMA-11 leading to significantly enhanced tumor-to-background contrast and reduced uptake in dose-limiting background organs (*22*). Because of the high clinical relevance, we introduced charged spacer moieties to our theranostic dual-modality platform, leading to a second generation of hybrid probes with improved imaging contrast. The insights investigated in this pharmacokinetic proof-of-concept study demonstrate a valuable progression aiming at clinical translation for better management of prostate cancer patients.

MATERIALS AND METHODS

Chemical Synthesis, Radiolabeling, Determination of Lipophilicity, and Serum Stability

The synthesis of the variants of Glu-urea-Lys-HBED-CC-IRDye800CW comprising a series of amino acid linker modifications was performed according to previously published protocols (*18*,*22–25*) (the supplemental materials available at http://jnm.snmjournals.org provide details on the synthesis and chemical structures of the compounds). $^{68}Ga^{3+}$ (half-life, 68 min; β^+, 89%; maximum $E_{\beta+}$, 1.9 MeV) was obtained from a ^{68}Ge/^{68}Ga generator based on a pyrogallol resin support, with details of compound characterization (radiolabeling, determination of lipophilicity, serum stability studies) provided in the supplemental materials (*26*).

In Vitro Evaluation

PSMA-positive LNCaP cells (CRL-1740; ATCC) and PSMA-negative PC-3 cells (CRL-1435; ATCC) were cultured in RPMI medium supplemented with 10% fetal calf serum and 2 mM L-glutamine (all from PAA). Cells were grown at 37°C in humidified air with 5% CO_2 and were harvested using trypsin-ethylenediaminetetraacetic acid (0.25% trypsin, 0.02% ethylenediaminetetraacetic acid; Invitrogen). Cell line authentication is regularly performed, and the LNCaP and PC-3 cell lines were authenticated on March 6, 2020. The competitive cell binding assay and internalization experiments were performed as described previously (*19*,*25*).

Biodistribution and Preclinical Proof of Concept

For the experimental tumor models, 5×10^6 cells of LNCaP or PC-3 (in 50% Matrigel; Becton Dickinson) were subcutaneously inoculated into the flank of 7- to 8-wk-old male BALB/c *nu/nu* mice (Charles River). For biodistribution studies, the ^{68}Ga-labeled compounds were injected into a tail vein (1–3 MBq [60 pmol, $n = 3$] and 30–50 MBq [500 pmol, $n = 3$]). At 1 and 2 h after injection, respectively, the animals were sacrificed. Organs of interest were dissected, blotted dry, and weighed. The radioactivity was measured using a γ-counter and calculated as percentage injected dose [%ID]/g. Optical imaging was performed with the Odyssey CLx system (excitation wavelength, 800 nm; LI-COR Biosciences). In an additional preclinical proof of concept ($n = 1$), mice were anesthetized (2% sevoflurane; Abbvie) and 0.5 nmol of the ^{68}Ga-labeled compound in 0.9% NaCl (pH 7) were injected into the tail vein. Preoperative PET imaging was performed with a PET scanner (Inveon PET; Siemens). For subsequent optical imaging to identify the tumor by fluorescence, mice were sacrificed after PET imaging and dissected tissue analyzed using the Odyssey CLx system (the supplemental materials provide details on the imaging protocol, software, image reconstruction, and procedure). All animal experiments were approved by the regional authorities *Regierungspräsidium Karlsruhe* and *Regierungspräsidium Freiburg* and complied with the current laws of the Federal Republic of Germany.

Statistical Aspects

Experiments were performed at least in triplicate, except for the proof-of-concept study ($n = 1$). Quantitative data are expressed as mean ± SD. The n values are given in the respective figure or table captions. If applicable, means were compared using the Student t test (Prism, version 8; GraphPad Software, Inc.). P values of less than 0.05 were considered statistically significant.

RESULTS

Synthesis, Radiolabeling, and Serum Stability

For this pharmacokinetic proof-of-concept study, Glu-urea-Lys-HBED-CC-IRDye800CW (tumor uptake 1 h after injection, 13.66 ± 3.73 %ID/g) was selected as an exemplary model core structure for our theranostic dual-modality platform for 2 main reasons. First, this compound has been preclinically proven to perform comparably to or even to outperform successfully established molecules such as PSMA-11 (tumor uptake 1 h after injection, 4.89 ± 1.34 %ID/g) or PSMA-617 (tumor uptake 1 h after injection, 8.47 ± 4.09 %ID/g) (*18*,*22*,*27*). Second, the choice of the structure previously comprising the bulky clinically relevant near-infrared dye IRDye800CW simplifies further clinical translation of the findings, since small molecules' biologic properties are typically strongly influenced when conjugated to a fluorescent dye. In a first step, charged linker moieties found to be favorable with respect to pharmacokinetic properties in previous studies were introduced combining solid-phase and classic organic synthesis strategies (Supplemental Figs. 1 and 2) (*18*,*22*). As the most promising candidate in former studies, the $(HE)_3$-motif was additionally inserted between the chelator and the fluorescent moiety to investigate the influence of linker positioning within the molecule (Supplemental Fig. 2) (*23*,*28*). The dye was conjugated to the precursor molecules as IRDye800CW-NHS-ester in the last step. A detailed description of

TABLE 1
Cell Binding and Internalization Data of Compounds

Compound	Specifically cell surface–bound*	Specifically internalized*	IC_{50} (nM)† Free ligands	$^{69/71}$Ga-labeled compounds
Glu-urea-Lys-$(HE)_1$-HBED-CC-IRDye800CW	3.00 ± 1.42	3.27 ± 1.83	28.41 ± 14.39	35.57 ± 22.83
Glu-urea-Lys-$(WE)_1$-HBED-CC-IRDye800CW	6.47 ± 3.69	13.77 ± 8.50	43.70 ± 14.12	56.80 ± 17.10
Glu-urea-Lys-$(HE)_3$-HBED-CC-IRDye800CW	8.30 ± 3.93	6.45 ± 3.36	51.29 ± 11.84	69.98 ± 22.88
Glu-urea-Lys-HBED-CC-$(HE)_3$-IRDye800CW	6.26 ± 1.49	3.70 ± 0.51	41.74 ± 18.26	52.21 ± 7.33

*^{68}Ga-labeled compounds. Specific cell uptake was determined by blockage using 500 μM 2-PMPA. Data are percentage applied radioactivity bound to 10^5 cells.

†Radioligand: ^{68}Ga-PSMA-10 (dissociation constant, 3.8 ± 1.8 nM (25); $c_{radioligand}$, 0.75 nM [c = concentration]).

Data are expressed as mean ± SD (n = 3). Affinity to PSMA and internalization properties of compounds were determined in vitro using PSMA-positive cells (LNCaP). For all compounds, PSMA-specific internalization was detected, as well as high binding affinity to PSMA (in low nanomolar range) not significantly dependent on complexation.

the synthetic strategies is provided in the supplemental materials. The final products were obtained in greater than 98% purity and their analytic data are summarized in Supplemental Figures 3 and 4 and Supplemental Tables 1 and 2. Lipophilicity, determined as log$D$ at pH 7.4 in n-octanol/phosphate-buffered saline, was found to be in the same range as the respective Glu-urea-Lys-HBED-CC-IRDye800CW reference compound with a $\log D_{pH\ 7.4}$ value of −2.21 ± 0.36 (Supplemental Table 1) (*18*). Radiolabeling with ^{68}Ga resulted in radiochemical yields greater than 99%, and the molar activities of the ^{68}Ga-labeled compounds were detected to be around 80–120 GBq/μmol (Supplemental Figs. 5–7). ^{68}Ga-Glu-urea-Lys-$(HE)_3$-HBED-CC-IRDye800CW was found to be stable in mouse and human serum up to 2 h.

PSMA-Specific Binding and Internalization Properties

High and specific affinity to PSMA in the nanomolar range was revealed for all tested compounds in competitive binding studies, and this affinity was not significantly complexation-dependent (Table 1; Supplemental Fig. 8). The introduction of $(HE)_1$- or tryptophane (W)-containing $(WE)_1$ motifs between the PSMA-binding motif and the chelator or of the $(HE)_3$ motif between the chelator and the fluorescent dye had no impact on binding properties as compared with the reference Glu-urea-Lys-HBED-CC-IRDye800CW (*18*). Interestingly, the $(HE)_3$ motif inserted between PSMA-binding unit and chelator moiety significantly reduced the affinity to PSMA (P = 0.024). Specific cell surface binding was detected for all tested dual-labeled probes (Table 1; Supplemental Fig. 9). Incorporating the $(WE)_1$ (P = 0.482) or $(HE)_3$ motif (P = 0.053) near the PSMA-binding motif resulted in the most pronounced specifically internalized fractions not significantly differing from the reference (*18*). In contrast, changing the intramolecular $(HE)_3$ motif position by inserting the linker between the chelator and the dye (P = 0.021) or introducing $(HE)_1$ as a linker structure next to the PSMA-binding motif (P = 0.021) revealed significantly reduced internalization properties (Table 1).

Specific Enrichment in Xenograft Tumors with Enhanced Contrast to Background Tissue

The impact of the introduction of charged amino acid linker motifs to Glu-urea-Lys-HBED-CC-IRDye800CW on in vivo specific PSMA targeting and accompanying background organ enrichment was further evaluated in biodistribution studies. ^{68}Ga-Glu-urea-Lys-$(HE)_3$-HBED-CC-IRDye800CW revealed a significantly increased, PSMA-specific tumor uptake in LNCaP xenograft tumors (7.59 ± 0.95 %ID/g, $P < 0.05$), compared with the incorporation of other motifs or intramolecular positioning of the $(HE)_3$ motif near the fluorescent dye at 1 h after injection (Figs. 1A and 1B; Supplemental Figure 10; Supplemental Tables 3–5). Although in comparison to the core structure, tumor uptake was significantly reduced for ^{68}Ga-Glu-urea-Lys-$(HE)_3$-HBED-CC-IRDye800CW (P = 0.031), it proved to be significantly increased when compared with ^{68}Ga-PSMA-11 (P = 0.047) or ^{68}Ga-PSMA-I&F (P = 0.045) and identical to ^{68}Ga-PSMA-617 (P = 0.735) (*17*,*22*,*27*). In addition, tracer uptake of ^{68}Ga-Glu-urea-Lys-$(HE)_3$-HBED-CC-IRDye800CW in nonmalignant tissue was significantly reduced to a minimum, with striking effects on spleen uptake, for example, which could be reduced from 38.12 ± 14.62 %ID/g to 3.47 ± 1.39 %ID/g (Fig. 1A; Supplemental Table 3) (*18*). From the series presented here, the introduction of the $(HE)_3$ motif near the PSMA-binding motif led to the highest tumor-to-background contrast. Noticeably, this compound even outperforms the core structure Glu-urea-Lys-HBED-CC-IRDye800CW with regard to tumor-to-background ratio (Supplemental Table 4). For all compounds, the renal pathway was identified to be the most likely elimination mechanism.

Additionally, to finalize the analysis of the pharmacokinetic properties of the favored compound ^{68}Ga-Glu-urea-Lys-$(HE)_3$-HBED-CC-IRDye800CW, biodistribution studies at 2 h after injection were conducted (Figs. 1C and 1D; Supplemental Table 6). Specific tumor accumulation was significantly reduced after injection of 60 pmol (3.10 ± 1.17 %ID/g) as compared with 1 h after injection (7.59 ± 0.95 %ID/g) (P = 0.007). Contemporaneously, the compound was strongly excreted from background tissue, resulting in remaining high tumor-to-background ratios up to 2 h after injection (Supplemental Table 6). Administration of higher doses of ^{68}Ga-Glu-urea-Lys-$(HE)_3$-HBED-CC-IRDye800CW (500 pmol) mainly confirmed the findings and even resulted in higher tumor-to-background ratios for muscle at 1 and 2 h after injection (Figs. 1C and 1D; Supplemental Tables 7 and 8).

Small-Animal PET and Optical Imaging

Subsequent small-animal PET studies with ^{68}Ga-Glu-urea-Lys-$(HE)_3$-HBED-CC-IRDye800CW confirmed strong tumor uptake in the LNCaP xenograft model accompanied by rapid clearance

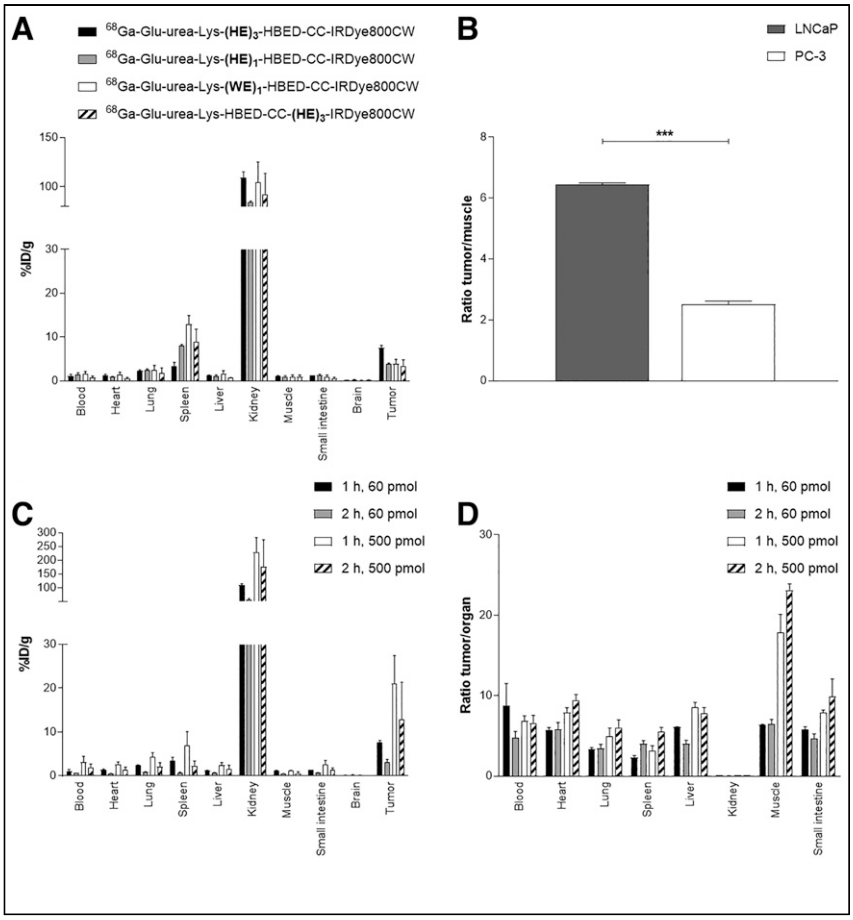

FIGURE 1. (A) Organ distribution of 60 pmol of ^{68}Ga-labeled compounds at 1 h after injection (LNCaP), with statistics shown in Supplemental Figure 10. (B) LNCaP in comparison to PC-3 tumor-to-muscle ratio of 60 pmol of ^{68}Ga-labeled Glu-urea-Lys-$(HE)_3$-HBED-CC-IRDye800CW 1 h after injection (***$P < 0.001$). (C and D) Organ distribution (C) and tumor-to-organ ratios (D) of 60 and 500 pmol of ^{68}Ga-labeled Glu-urea-Lys-$(HE)_3$-HBED-CC-IRDye800CW at 1 and 2 h after injection in LNCaP tumor–bearing BALB/c *nu/nu* mice. Data are expressed as mean %ID/g tissue ± SD ($n = 3$).

from nonmalignant tissue, resulting in high imaging contrasts at early time points after injection (Figs. 2A–2D). High PSMA specificity was proven in vivo because no measurable uptake was observed in PSMA-negative PC-3 xenografts (Fig. 2B). The corresponding time–activity curves of the dynamic PET scan up to 60 min after injection demonstrate rapid clearance from off-target tissue (muscle, liver, heart) but continuous accumulation in bladder and kidney due to the renal pathway of excretion (Fig. 2C).

In fluorescence imaging, ^{68}Ga-labeled Glu-urea-Lys-$(HE)_3$-HBED-CC-IRDye800CW obtained high tumor uptake, resulting in excellent tumor visualization and strong tumor-to-background contrast (Fig. 3; Supplemental Figs. 11 and 12). Additionally, the renal excretion pathway and the significantly reduced spleen uptake based on radioactivity was fluorescently confirmed.

DISCUSSION

The development of dual-modality probes for preoperative imaging and intraoperative guidance (radioguidance or fluorescence guidance) specifically targeting PSMA represents a promising new strategy in the diagnosis and therapy of PCa. The improved detection of tumor tissue supported by both a γ-signal and a fluorescent dye might overcome current surgical limitations. Therefore, a novel class of dual-labeled low-molecular-weight PSMA inhibitors has recently been developed, thereby successfully demonstrating their feasibility for clinical translation in preclinical proof-of-concept studies (*16–18*). In particular, a specific and sufficiently high tumor uptake combined with a fast pharmacokinetic profile resulting in high tumor-to-background contrast at early time points after injection challenges low-molecular-weight hybrid tracer development. ^{68}Ga-Glu-urea-Lys-HBED-CC-IRDye800CW was the first PSMA-targeting low-molecular-weight hybrid probe characterized by a 3-fold increased tumor uptake compared with the parental molecule PSMA-11 while preserving a fast pharmacokinetic profile.

Nevertheless, like other peptidomimetic PSMA inhibitors, this dual-modality approach results in excretion via the renal pathway and accumulation in nonmalignant tissue (spleen). Probe enrichment close to the surgical field might hamper specific lesion detection, particularly when close to the urinary system. Additionally, nonmalignant accumulation might be of concern regarding toxicity issues during clinical translation of this approach.

To address this limitation, our study found a rational hybrid molecule design to be a promising tool to accelerate the pharmacokinetic profile while preserving high tumor uptake. In particular, introduction of spacer moieties comprising (HE) proved favorable to modulate the biodistribution profile of Affibody molecules and peptidomimetic inhibitors, thereby improving tumor-to-background contrast and potential uptake in dose-limiting nonmalignant tissue (*21–23*).

In this study, rational linker design was applied to the peptidomimetic hybrid molecule Glu-urea-Lys-HBED-CC-IRDye800CW, the current lead of our theranostic dual-modality platform. Because of its favorable characteristics (high specific tumor uptake, fast pharmacokinetic properties) and successfully incorporated clinically relevant near-infrared dye (simplified clinical translation of pharmacokinetic study findings), it was designated for a further proof-of-concept pharmacokinetic modulation (*18*). The chemical motifs $(HE)_1$, $(HE)_3$, and $(WE)_1$ found to be beneficial in previous studies were selected for this approach (*21–23*).

The binding affinities of all second-generation compounds resulting from the present study were in the low-nanomolar range, indicating the selected linker motifs to have a negligible functional impact. Nevertheless, inserting the (HE) motif as a triplicate between the PSMA-binding motif and the chelator slightly reduces PSMA affinity. Although a single charged or lipophilic motif is tolerated in terms of affinity, motif repetitions might hamper the advantageous interactions of the chelator HBED-CC with the arene-binding side of the PSMA-binding pocket (*29*). Specific internalization of all modifications was observed to be highest for the

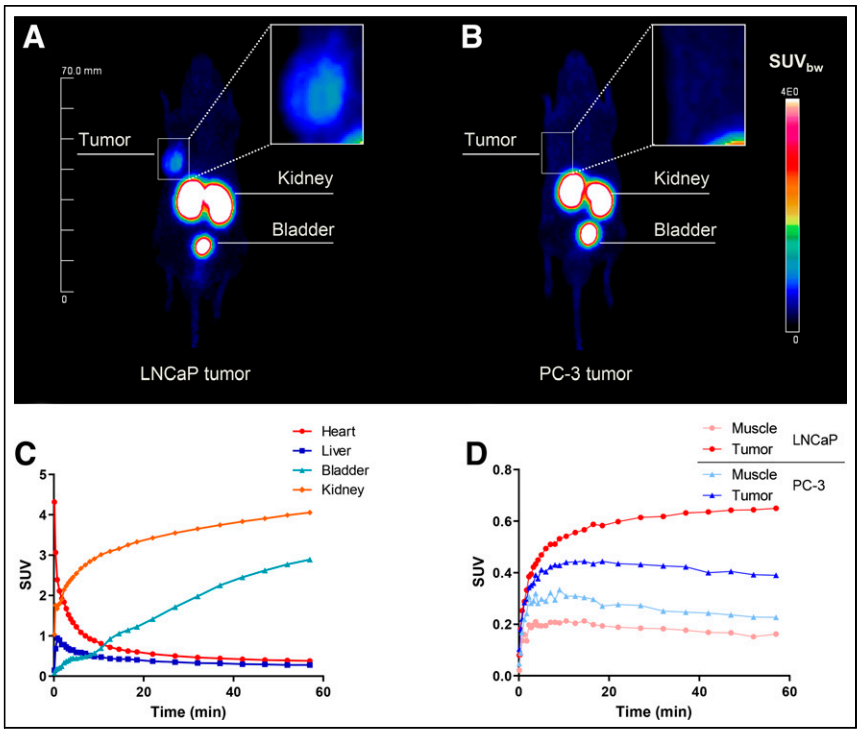

FIGURE 2. (A and B) Whole-body maximum-intensity projections with tumor magnifications of 0.5 nmol of ^{68}Ga-labeled Glu-urea-Lys-$(HE)_3$-HBED-CC-IRDye800CW (~50 MBq) in LNCaP (A) and PC-3 (B) tumor–bearing BALB/c *nu/nu* mice (right flank) 120 min after injection obtained from small-animal PET imaging (n = 1; 1 animal was used for each cell line LNCaP and PC-3, respectively). (C and D) Corresponding time–activity curves for background organs (C) and for tumor and muscle (D).

tryptophan-containing motif located close to the PSMA-binding motif, hypothetically exploiting supportive lipophilic interactions in the PSMA funnel (*30*).

However, the determined advantageous in vitro properties of $(HE)_1$ and $(WE)_1$ motif introduction did not result in an increased tumor uptake. Although $(HE)_1$ and $(WE)_1$ located between the PSMA-binding unit and the radiometal chelator significantly enhanced tumor uptake in previous findings (*22*), the effect could not be demonstrated in this study. Strikingly, including the $(HE)_3$ motif at the same intramolecular location resulted in a strongly improved background organ enrichment profile of the hybrid molecule at early time points after injection (1 h after injection). In particular, spleen uptake was reduced by a factor of 11 when compared with the parental structure ^{68}Ga-Glu-urea-Lys-HBED-CC-IRDye800CW, matching findings of earlier studies (*22*). In addition, this modification revealed the highest tumor-to-background ratios to relevant nonmalignant tissue of all tested compounds, including the parental structure. The resulting tumor uptake was significantly higher than for any of the other modified variants of this study, and previously reported compounds such as PSMA-11 and PSMA-I&F—not, however, exceeding the core structure Glu-urea-Lys-HBED-CC-IRDye800CW and PSMA-617 (*17*,*19*,*27*). Accordingly, it can be concluded that the novel compound features superior characteristics in terms of tumor uptake and tumor-to-background contrast warranting further investigation.

Thus, the exact intramolecular position of $(HE)_3$ was found to be highly crucial, because an introduction on a different location in the molecule results in significantly reduced or even negative effects on background organ enrichment and tumor uptake. The introduction of $(HE)_3$ near the PSMA-binding motif was found to noticeably influence the spleen uptake, for instance, as is in line with previous studies (*22*).

The improved background organ enrichment profile of the novel hybrid molecule ^{68}Ga-Glu-urea-Lys-$(HE)_3$-HBED-CC-IRDye
800CW was accompanied by a significantly accelerated excretion via the renal pathway by means of reduced kidney enrichment as compared with the parental structure ^{68}Ga-Glu-urea-Lys-HBED-CC-IRDye800CW, leading to high tumor-to-background-contrast as early as 1 h after injection, which proved persistent up to 2 h after injection (*18*). Surprisingly, at 1 h after

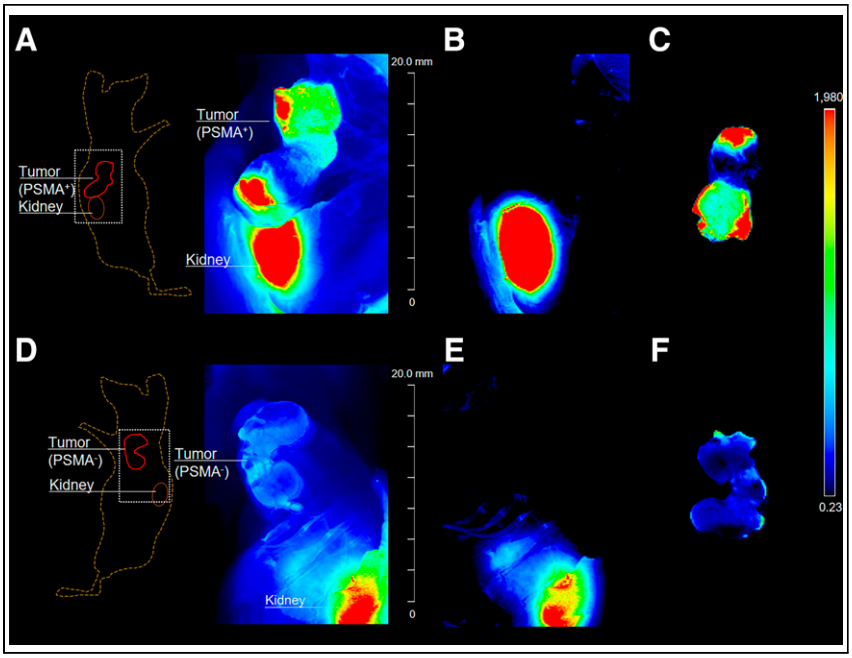

FIGURE 3. Optical imaging after injection of 0.5 nmol of ^{68}Ga-labeled Glu-urea-Lys-$(HE)_3$-HBED-CC-IRDye800CW in LNCaP (A–C) and PC-3 (D–F) tumor–bearing BALB/c *nu/nu* mice (n = 1; 1 animal was used for each cell line LNCaP and PC-3, respectively). Mice were sacrificed 2 h after injection after PET imaging, and fluorescence was detected with Odyssey CLx system (excitation wavelength, 800 nm). Fluorescence intensity is presented in heat-map coloring. (A and D) Skin covering subcutaneous xenograft tumors was removed, and imaging was performed to locate tumor. (B and E) Tumor tissue was resected and another scan performed to ensure complete tumor tissue removal. (C and F) Fluorescence signal of resected tumors is presented. Tissue lying on surface of imaging system during fluorescence detection explains small artifacts in fluorescence images.

injection, the high tumor-to-background contrast manifested about 60 min earlier for the pharmacokinetic-improved compound than for the parental compound. This earlier manifestation is caused by a dramatically minimized enrichment in nonmalignant tissue leading to a 2.0-fold higher tumor-to-blood ratio and a 1.6-fold higher tumor-to-muscle ratio at early time points after injection of 60 pmol. Consequently, increased contrast in the surgical field can be expected from these data, encouraging further clinical translation. Since other dyes are also being discussed in terms of stability, brightness, or tissue penetration, for example, further studies might identify the ideal combination finally representing the lead second-generation PSMA-targeting hybrid probe.

CONCLUSION

This study found rational linker design to be a powerful tool in hybrid molecule development, leading to a novel generation of PSMA-targeting peptidomimetic hybrid molecules with a significantly improved pharmacokinetic profile. With fast elimination and subsequent reduced enrichment in nonmalignant tissue, this approach addresses the highly disruptive factor of background accumulation during surgical resection while preserving a high PSMA-specific tumor uptake. The pharmacokinetic modification strategy uncovered in this study offers extensive utility in the future discovery and development of targeted peptidomimetic hybrid agents.

DISCLOSURE

Financial support was received through the VIP+ grant VP00130, Federal Ministry of Education and Research (BMBF), Germany. Martin Schäfer, Ulrike Bauder-Wüst, Uwe Haberkorn, Matthias Eder, Klaus Kopka, and Ann-Christin Eder hold patent rights on dual-labeled PSMA inhibitors. No other potential conflict of interest relevant to this article was reported.

KEY POINTS

QUESTION: Is the tool of rational linker design suitable to improve the pharmacokinetic profile and elimination rate in peptidomimetic hybrid molecule development?

PERTINENT FINDINGS: This preclinical proof-of-concept study found rational linker design to be a valuable tool to selectively affect the pharmacokinetic profile and elimination rate of PSMA-targeting peptidomimetic hybrid molecules. Introduction of a designated sequence of amino acids significantly reduced enrichment in nonmalignant tissue to a minimum, thereby also enhancing the elimination profile while preserving a high specific tumor uptake.

IMPLICATIONS FOR PATIENT CARE: Background-organ accumulation of novel hybrid molecules in, for example, the surgical field represents one of the main challenges in hybrid molecule development. The study findings introduce a tool to overcome these limitations and further advance discovery in novel image-guided surgery approaches for clinical translation.

REFERENCES

1. Cornford P, van den Bergh RCN, Briers E, et al. EAU-EANM-ESTRO-ESUR-SIOG guidelines on prostate cancer. Part II-2020 update: treatment of relapsing and metastatic prostate cancer. *Eur Urol.* 2021;79:263–282.
2. Weckermann D, Dorn R, Trefz M, Wagner T, Wawroschek F, Harzmann R. Sentinel lymph node dissection for prostate cancer: experience with more than 1,000 patients. *J Urol.* 2007;177:916–920.
3. Mattei A, Fuechsel FG, Bhatta Dhar N, et al. The template of the primary lymphatic landing sites of the prostate should be revisited: results of a multimodality mapping study. *Eur Urol.* 2008;53:118–125.
4. Yossepowitch O, Briganti A, Eastham JA, et al. Positive surgical margins after radical prostatectomy: a systematic review and contemporary update. *Eur Urol.* 2014;65:303–313.
5. Stephenson AJ, Eggener SE, Hernandez AV, et al. Do margins matter? The influence of positive surgical margins on prostate cancer-specific mortality. *Eur Urol.* 2014;65:675–680.
6. Munbauhal G, Seisen T, Gomez FD, et al. Current perspectives of sentinel lymph node dissection at the time of radical surgery for prostate cancer. *Cancer Treat Rev.* 2016;50:228–239.
7. Kiss B, Thoeny HC, Studer UE. Current status of lymph node imaging in bladder and prostate cancer. *Urology.* 2016;96:1–7.
8. van der Poel HG, Buckle T, Brouwer OR, Valdes Olmos RA, van Leeuwen FW. Intraoperative laparoscopic fluorescence guidance to the sentinel lymph node in prostate cancer patients: clinical proof of concept of an integrated functional imaging approach using a multimodal tracer. *Eur Urol.* 2011;60:826–833.
9. Brouwer OR, Buckle T, Vermeeren L, et al. Comparing the hybrid fluorescent-radioactive tracer indocyanine green-^{99m}Tc-nanocolloid with ^{99m}Tc-nanocolloid for sentinel node identification: a validation study using lymphoscintigraphy and SPECT/CT. *J Nucl Med.* 2012;53:1034–1040.
10. KleinJan GH, van den Berg NS, de Jong J, et al. Multimodal hybrid imaging agents for sentinel node mapping as a means to (re)connect nuclear medicine to advances made in robot-assisted surgery. *Eur J Nucl Med Mol Imaging.* 2016;43:1278–1287.
11. Silver DA, Pellicer I, Fair WR, Heston WD, Cordon-Cardo C. Prostate-specific membrane antigen expression in normal and malignant human tissues. *Clin Cancer Res.* 1997;3:81–85.
12. Wright GL Jr, Haley C, Beckett ML, Schellhammer PF. Expression of prostate-specific membrane antigen in normal, benign, and malignant prostate tissues. *Urol Oncol.* 1995;1:18–28.
13. Sweat SD, Pacelli A, Murphy GP, Bostwick DG. Prostate-specific membrane antigen expression is greatest in prostate adenocarcinoma and lymph node metastases. *Urology.* 1998;52:637–640.
14. Minner S, Wittmer C, Graefen M, et al. High level PSMA expression is associated with early PSA recurrence in surgically treated prostate cancer. *Prostate.* 2011;71:281–288.
15. Lütje S, Rijpkema M, Franssen GM, et al. Dual-modality image-guided surgery of prostate cancer with a radiolabeled fluorescent anti-PSMA monoclonal antibody. *J Nucl Med.* 2014;55:995–1001.
16. Banerjee SR, Pullambhatla M, Byun Y, et al. Sequential SPECT and optical imaging of experimental models of prostate cancer with a dual modality inhibitor of the prostate-specific membrane antigen. *Angew Chem Int Ed Engl.* 2011;50:9167–9170.
17. Schottelius M, Wurzer A, Wissmiller K, et al. Synthesis and preclinical characterization of the PSMA-targeted hybrid tracer PSMA-I&F for nuclear and fluorescence imaging of prostate cancer. *J Nucl Med.* 2019;60:71–78.
18. Baranski AC, Schafer M, Bauder-Wust U, et al. PSMA-11-derived dual-labeled PSMA inhibitors for preoperative PET imaging and precise fluorescence-guided surgery of prostate cancer. *J Nucl Med.* 2018;59:639–645.
19. Eder M, Schafer M, Bauder-Wust U, et al. ^{68}Ga-complex lipophilicity and the targeting property of a urea-based PSMA inhibitor for PET imaging. *Bioconjug Chem.* 2012;23:688–697.
20. Hope TA, Aggarwal R, Chee B, et al. Impact of ^{68}Ga-PSMA-11 PET on management in patients with biochemically recurrent prostate cancer. *J Nucl Med.* 2017;58:1956–1961.
21. Hofstrom C, Orlova A, Altai M, Wangsell F, Graslund T, Tolmachev V. Use of a HEHEHE purification tag instead of a hexahistidine tag improves biodistribution of Affibody molecules site-specifically labeled with ^{99m}Tc, ^{111}In, and ^{125}I. *J Med Chem.* 2011;54:3817–3826.
22. Baranski AC, Schafer M, Bauder-Wust U, et al. Improving the imaging contrast of ^{68}Ga-PSMA-11 by targeted linker design: charged spacer moieties enhance the pharmacokinetic properties. *Bioconjug Chem.* 2017;28:2485–2492.
23. Eder M, Löhr T, Bauder-Wüst U, et al. Pharmacokinetic properties of peptidic radiopharmaceuticals: reduced uptake of (EH)3-conjugates in important organs. *J Nucl Med.* 2013;54:1327–1330.
24. Eder M, Wangler B, Knackmuss S, et al. Tetrafluorophenolate of HBED-CC: a versatile conjugation agent for ^{68}Ga-labeled small recombinant antibodies. *Eur J Nucl Med Mol Imaging.* 2008;35:1878–1886.

25. Schafer M, Bauder-Wust U, Leotta K, et al. A dimerized urea-based inhibitor of the prostate-specific membrane antigen for ^{68}Ga-PET imaging of prostate cancer. *EJNMMI Res.* 2012;2:23.
26. Schuhmacher J, Maier-Borst W. A new Ge-68/Ga-68 radioisotope generator system for production of Ga-68 in dilute HCl. *Int J Appl Radiat Isot.* 1981;32:31–36.
27. Benešová M, Schafer M, Bauder-Wust U, et al. Preclinical evaluation of a tailor-made DOTA-conjugated PSMA inhibitor with optimized linker moiety for imaging and endoradiotherapy of prostate cancer. *J Nucl Med.* 2015;56:914–920.
28. Liolios C, Schafer M, Haberkorn U, Eder M, Kopka K. Novel bispecific PSMA/GRPr targeting radioligands with optimized pharmacokinetics for improved PET imaging of prostate cancer. *Bioconjug Chem.* 2016;27:737–751.
29. Zhang AX, Murelli RP, Barinka C, et al. A remote arene-binding site on prostate specific membrane antigen revealed by antibody-recruiting small molecules. *J Am Chem Soc.* 2010;132:12711–12716.
30. Mesters JR, Barinka C, Li W, et al. Structure of glutamate carboxypeptidase II, a drug target in neuronal damage and prostate cancer. *EMBO J.* 2006;25:1375–1384.